2018 IEEE 59th International Scientific Conference on Power and Electrical Engineering of Riga Technical University (RTUCON)

An Indirect Model Predictive Current Control (CCS-MPC) for Grid-Connected Single-Phase Three-Level NPC Quasi-Z-Source PV Inverter

Sergio Pires Pimentel[12], Oleksandr Husev[13], Dmitri Vinnikov[1], Carlos Roncero-Clemente[4], and Serhii Stepenko[13]
[1]Power Electronics Group, Department of Electrical Power Engineering and Mechatronics
Tallinn University of Technology (TalTech), Tallinn, Estonia
Email: sergio.pimentel@ieee.org, oleksandr.husev@ieee.org, dmitri.vinnikov@ieee.org
[2]Federal University of Goias (UFG), Goiania, Brazil
[3]Chernihiv National University of Technology, Chernihiv, Ukraine
[4]Universidad de Extremadura, Badajoz, Spain

***Abstract*—In this paper, a model predictive control (MPC) based on the indirect continuous-control set (CCS) is proposed for regulating the grid current waveform provided by a PV grid-connected single-phase inverter. It involves a three-level NPC quasi-Z-source (3L-NPC qZS) inverter, an only-string PV array, and a LCL output filter. From a finite set of modulation index values, the proposed indirect CCS-MPC current control selects one of them for an external fixed switching frequency driver based on LS-PWM strategy. An issue regarding cost function composition and modulation index regulation is also proposed for improvement of transient and steady-state responses. Simulations results from a PSCAD/EMTDC model are presented and discussed. Even limited by a fixed switching frequency, obtained results demonstrate: an acceptable accuracy of the proposed system model; and a robustness of the evaluated indirect CCS-MPC grid current method under some external perturbation conditions.**

Keywords—Predictive Control; Discrete-time Systems; Power Electronics; Photovoltaic Systems; Distributed Power Generation.

I. INTRODUCTION

It is notorious how grid-connected PV systems have becoming more popular for over last years, especially in terms ac low-voltage single-phase power systems. There are a lot of well-known features regarding their dynamics, benefits and drawbacks related to power converters operation and grid utility stability [1], [2].

This paper focus on the improvement and controllability of grid current waveform injected into grid-utility by a distributed generation system based on PV arrays. For that, a feedback system based on model predictive control (MPC) had been chosen instead of conventional methodologies (for instance, linear and PR controllers) because of its improvement on the robustness of overall feedback control operation and its relative simplicity for simulation and experimental verifications.

Other benefits from the adoption of MPC with power converters are described in [3], [4] as: an elevation of the power capability from a converter; a reduction of current distortions and hardware requirements; an achievement of very fast transient responses; and a reliable feedback operation within safe operating area constraints.

According to [5]-[7], MPC methodology has basically two main different approaches in terms of power converters control: continuous-control set MPC (CCS-MPC); and finite-control set MPC (FCS-MPC). Indirect and direct MPC, respectively. The main difference between them is related to the elaboration of all gate signals that would be provided to power converters. Basically, the direct MPC (or FCS-MPC) determines an exact switching state vector (from a finite set of possible combinations) that would be directly applied to switching devices and without any additional stage for a modulation strategy elaboration. Otherwise, the indirect MPC (or CCS-MPC) provides a specific value of modulation index (from a selected range of deviation) that would be applied to gate signals by any modulation strategy.

Based on this aspect, a direct MPC could provide higher switching commutations of power converters but it requires a more complex hardware implementation. And an indirect MPC could be easily applied to available power converters and it would be limited by the switching frequency defined to selected modulation strategy. On this paper, the indirect MPC was chosen to provide a better feedback control operation of an already implemented single-phase power inverter for experimental verifications.

The main contributions from this paper are: an accurate discrete-time model from ac-side of grid-connected inverter with a LCL output filter in terms of steady-state LTI MIMO notation; a step-by-step description of proposed indirect CCS-MPC method and its main operation features; a simulation model of the proposed method built on PSCAD/EMTDC; an analysis of the proposed method for regulating the grid current provided by a single-phase three-level NPC quasi-Z-Source (3L-NPC qZS) inverter in PV grid-connected systems; and a discussion regarding proposal of cost function composition for improving robustness capability on both steady-state and transient-time domains. Next sections describe all of them, followed by a discussion of results and conclusions.

978-1-5386-6903-7/18/$31.00 ©2018 IEEE

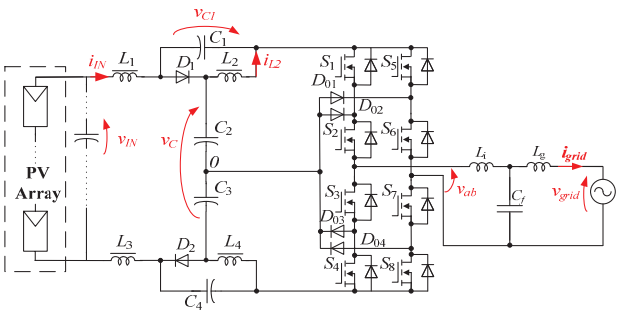

Fig. 1. PV grid-connected system with single-phase 3L-NPC qZS inverter.

TABLE I.
CONSIDERED SPECIFICATIONS FOR THE CASE OF STUDY

Capacitances from capacitors C_1 and C_4	2.70 mF
Capacitances from capacitors C_2 and C_3	1.47 mF
Inductances from inductors L_1 and L_3	400 µH
Inductances from inductors L_2 and L_4	200 µH
First filter inductance L_i (inverter) – **L**CL	440 µH
Filter capacitance C_f – L**C**L	15.47 µF
Second filter inductance L_g (grid) – LC**L**	220 µH
Grid-utility nominal voltage (L1-L0)	230 V
Grid-utility fundamental frequency	50 Hz
Switching frequency (MOSFET devices)	100 kHz
Sampling frequency (DAC & ADC converters)	8 kHz

II. CASE OF STUDY

The case of study covered by this work is presented in Fig. 1. As expected, it consists of a single-phase 3L-NPC qZS inverter fed by a 3 kWp PV array and connected to grid-utility by an LCL filter tuned at 2.7 kHz [8]. Other specification values from system shown in Fig. 1 are presented in Tab. I.

Power semiconductors devices from Fig. 1 have a switching pattern defined by a modulation strategy based on Level-Shift Modified PWM (LS-PWM) with Phase-Disposition (PD) of double carrier waveforms (5 levels). According to [9], this specific modulation strategy is also combined with Maximum Constant Boost Control (MCBC) method for guaranteeing a suitable Shoot-Through (ST) duty cycle to dc-side of 3L-NPC qZS inverter topology.

III. PROPOSED INDIRECT CCS-MPC

The case of study covered by this work is presented in Fig. 1. As expected, it consists of a single-phase 3L-NPC qZS inverter fed by a 3 kWp PV array and connected to grid-utility by an LCL filter tuned at 2.7 kHz [8]. Other specification values from system shown in Fig. 1 are presented in Tab. I.

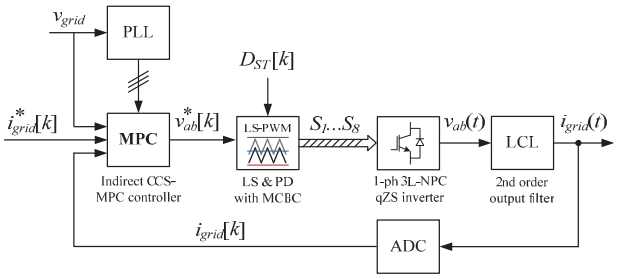

Fig. 2. Grid current control loop and proposed indirect CCS-MPC controller.

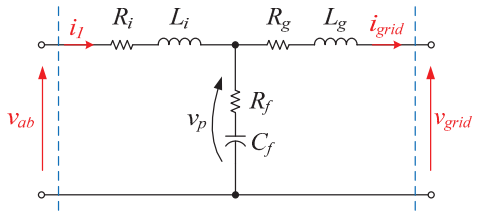

Fig. 3. Considered model for the LCL output filter and grid-connection.

For the system of Fig. 1, the block diagram of proposed indirect current CCS-MPC method is presented in Fig. 2. It provides a voltage reference v_{ab}* to 3L-NPC qZS inverter based on grid voltage v_{grid}, grid current i_{grid}, and grid current reference i_{grid}*.

As the grid voltage v_{grid} available at PCC (Point of Common Coupling) is considered as an input signal to control diagram from Fig. 2, the proposed indirect CCS-MPC method can follow the dynamical operation of grid-utility. It means that none electrical model from grid-utility power lines is required and its dynamics can be tracked just by measuring the grid voltage v_{grid} at PCC. In order to achieve a better dynamical tracking, the proposed method can apply an external PLL (phase locking) algorithm for providing: grid voltage frequency f_{grid}; grid voltage angle θ_{grid}; and grid voltage peak v^{pk}_{grid} at fundamental frequency. Next four subsections describe the main aspects of proposed indirect CCS-MPC method regarding the v_{ab}* elaboration.

A. Internal dynamic model

The internal dynamic model (IDM) that emulates the dynamics of system presented in Fig. 1 regarding the grid current control can be represented by the circuit exhibits in Fig. 3. Additional passive elements were considered for evaluating their effects on the relative stability of system.

The MIMO system presented in Fig. 3 corresponds to an LTI system and it can be described as follow in terms of steady-state equations (under continuous-time domain).

$$\mathbf{x}(t) = [\, i_1(t) \quad i_{grid}(t) \quad v_{Cf}(t) \,]^T \tag{1}$$

$$\mathbf{u}(t) = [\, v_{ab}(t) \quad v_{grid}(t) \,]^T \tag{2}$$

$$\mathbf{x}^{\cdot}(t) = \mathbf{F}\cdot\mathbf{x}(t) + \mathbf{G}\cdot\mathbf{u}(t) \tag{3}$$

$$\mathbf{F} = \begin{vmatrix} -(R_i + R_f)/L_i & R_f/L_i & -1/L_i \\ R_f/L_g & -(R_g + R_f)/L_g & 1/L_g \\ 1/C_f & -1/C_f & 0 \end{vmatrix} \tag{4}$$

$$\mathbf{G} = \begin{vmatrix} 1/L_i & 0 \\ 0 & -1/L_g \\ 0 & 0 \end{vmatrix} \tag{5}$$

It is possible to determine an equivalent discrete-time model from the correspond continuous-time domain model shown in (3) by means of (6), (7), and (8) [4]. By that, it is possible to predict the state of vector $\mathbf{x}[k+1]$ which corresponds to estimated values on variables from state vector $\mathbf{x}[k]$ after passing the next sampling period T_s [10].

$$\mathbf{x}[k+1] = \mathbf{A}\cdot\mathbf{x}[k] + \mathbf{B}\cdot\mathbf{u}[k] \tag{6}$$

$$\mathbf{A} = \exp(\mathbf{F}\cdot T_s) \tag{7}$$

$$\mathbf{B} = [\,(\mathbf{A} - \mathbf{I})\cdot\mathbf{G}\,]^{-1}\cdot\mathbf{F} \tag{8}$$

For the case $R_i = R_g = R_f = 0.1\ \Omega$, and the specifications from Tab. I, the properly IDM of system presented in Fig. 3 and related to the particular case of study shown in Fig. 1 can be described by (6)-(10).

$$\mathbf{A} = \begin{vmatrix} -0.23094 & 1.19070 & -0.09902 \\ 0.59533 & 0.36913 & 0.05159 \\ 1.40820 & -1.46730 & -0.80130 \end{vmatrix} \tag{9}$$

$$\mathbf{B} = \begin{vmatrix} 0.25095 & -0.15193 \\ 0.15193 & -0.20351 \\ 1.19590 & 0.60536 \end{vmatrix} \tag{10}$$

B. Cost function and constraints

A predefined cost function can be applied to minimize the difference among reference and several predicted values over a period of consecutive sampling-time steps.

The cost function $J\,[m, d]$ described in (11) was applied in the proposed indirect current CCS-MPC method.

$$J\,[m, d] = \{\, i_{grid}^{*}[m] - i_{pred}\,[m, d]\,\}^2 \quad (m \geq k) \tag{11}$$

The function $J\,[m, d]$ quantizes estimations of different squared current errors. And each of those estimations can be associated with a possible scenario d, which could occur at instant mT_s and result on a predictive grid current $i_{pred}\,[m, d]$.

As the any indirect MPC control method is associated with a fixed switching frequency, a finite number of scenarios was considered for this work. The proposed scenarios d and respective voltage deviations $\Delta v_{ab}^{*}[d, m]$ are described in Tab. II. Based on them, a specific possible reference voltage $v_{ab}^{*}[d, m]$ during cost function evaluation is also shown in (12).

$$v_{ab}^{*}[d, m] = v_{grid}[m] + \Delta v_{ab}^{*}[d, m] \quad (m \geq k) \tag{12}$$

TABLE II.
SCENARIOS AND VOLTAGE DEVIATIONS FOR COST FUNCTION J

Scenario	Evaluation band	$\Delta v_{ab}^{*}[d, m]$	$\Delta v_{ab,pu}^{*}[d, m]$
$d = 1$	–100.0%	–40.0 V	–10.0 pu
$d = 2$	–75.0%	–30.0 V	–7.5 pu
$d = 3$	–50.0%	–20.0 V	–5.0 pu
$d = 4$	–25.0%	–10.0 V	–2.5 pu
$d = 5$	null	0.0 V	0.0 pu
$d = 6$	+25.0%	+10.0 V	+2.5 pu
$d = 7$	+50.0%	+20.0 V	+5.0 pu
$d = 8$	+75.0%	+30.0 V	+7.5 pu
$d = 9$	+100.0%	+40.0 V	+10.0 pu

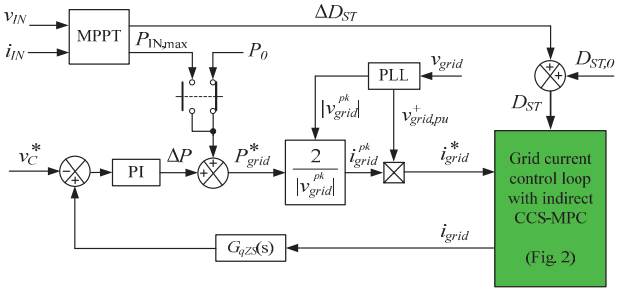

Fig. 4. External voltage control loop that also provides reference i_{grid}^{*}.

C. Optimization stage and receding horizon

Based on [3], [4], the considered optimization stage is described in (13). The function d_p[m] corresponds to the minimum value among all possible scenarios evaluated in (11). Then, by means of (14), the selected predictive deviation $d_p[m]$ determines the reference voltage $v_{ab}^{*}[m]$ that should be performed by the 3L-NPC qZS inverter.

$$d_p[m] = \arg\min J\,[m, d] \tag{13}$$

$$v_{ab}^{*}[m] = v_{ab}^{*}\{d_p[m], m\} \tag{14}$$

The amount of m consecutive terms involved by a time horizon evaluation through (11-14) could be defined as the length of receding horizon from the MPC method. In this work, in order to reduce the effect of sampling time-delay and digital signal processing on cost function J composition, the receding horizon was adopted as $m = (k + 2)$ [11], [12].

D. External voltage control loop

The proposed indirect CCS-MPC method from Fig. 2 could be associated with an external dc-link voltage control loop that would affect the overall absolute and relative stability of the feedback control system. Fig. 4 exhibits a possible external voltage control loop for the indirect MPC control method proposed by this work. Its main features as well the voltage

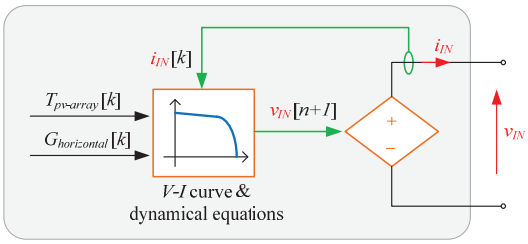

Fig. 5. General overview of applied PV dynamical model proposed in [14].

controller tuning procedure were described in [13] considering the same case of study shown in Fig. 1.

The efficacy operation of the proposed indirect CCS-MPC method is also based on the reference current i_{grid}* which is provided by the external voltage control loop. At the same time, the second loop assumes that first one would be able to provide a current i_{grid} as closed as possible to its reference. Results that exemplifies those mutual dynamical operations between outer and inner loops are discussed as follow.

IV. Results

The performance of proposed grid current indirect CCSMPC control method was evaluated by a simulation model built on PSCAD/EMTDC. Besides the system specifications declared on previous sections, simulation model was also settled with two more specific time intervals in order to provide a better accuracy of results.

For that reason, all simulations were performed considering a time-step of 0.05 µs and graphs have 5.00 µs of resolution. Both values were defined based on the already-known power switching time-period (10.00 µs, according to Tab. I).

A. Dynamic PV array model

This work applied an accurate PV dynamical model proposed in [14] for PSCAD/EMTDC that it can properly to follow both expected P-V and I-V characteristics curves, to specify the MPP (maximum power point) according to external meteorological conditions, and also to provide transient time responses similar to real PV systems.

It was considered a PV array composed by only one string with same PV modules BISOL BMU-255 [15]. According to the technical specifications of PV module and single-phase grid-connection requirements presented in Tab. I, a PV array model was built on PSCAD for a PV string composed by 12 PV modules (1x12). Fig. 5 presents a general overview of model built on PSCAD and adjusted according to [15].

Basically, the operation of model shown in Fig. 5 can be described as follows in closed loop mode. From the PV model perspective, an expected value of the next short-time dc output voltage v_{IN} is transferred to its terminals according to actual measured values of solar irradiance $G_{horizontal}$ (in W/m^2), PV cell temperature $T_{pv-array}$ (in °C), and its dc output current i_{IN} (in p.u.). This last one could be even replaced by a reference current value during an open loop evaluation.

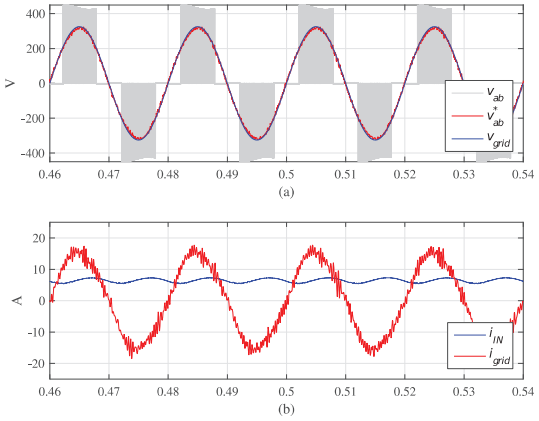

Fig. 6. Voltage and current waveforms during steady-state operation without dc-link voltage control and under low input power condition.

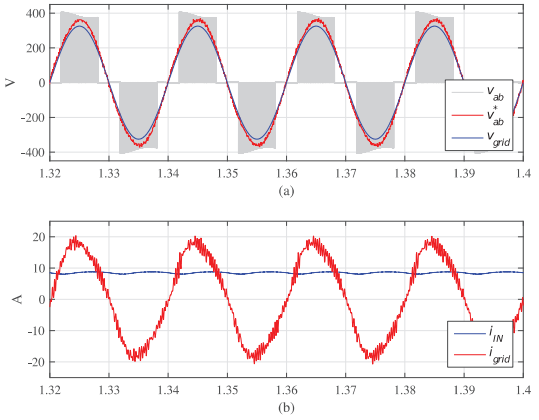

Fig. 7. Voltage and current waveforms during steady-state operation with a well tuned dc-link voltage control and under maximum input power condition.

B. Short-time observation window

A short-time observation window (four cycles of fundamental frequency) was considered to verify the system performance during a steady-state operation condition. Then, two different conditions were considered: low input power level without any dc-link voltage control regulation (Figs. 6 and 8); and maximum input power level with tuned dc-link voltage control (Figs. 7 and 9).

From those curves, it can be noticed the addition of intentional deviations provided by the proposed indirect CCS-MPC method. By them, a sequence of deviations added to reference voltage v_{ab}* and around the grid voltage v_{grid} allowed the grid current i_{grid} regulation according to its reference i_{grid}*. Besides, the regulation actions on dc-link voltage provided an operation of power converter with higher values of modulation index and, for that reason, some current distortions were observed. Under a maximum input power level, ripple oscillations on input current were lower than previously presented.

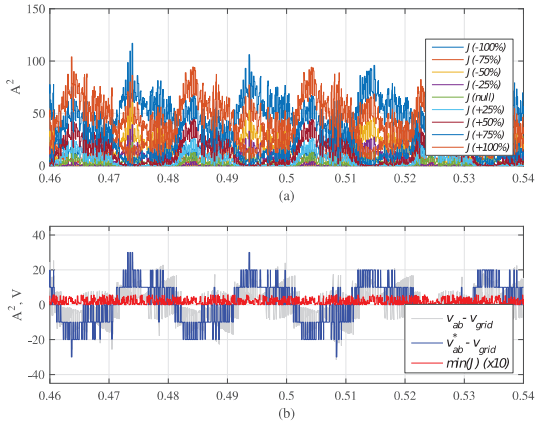

Fig. 8. Cost function components and voltage deviations related to Fig. 6 - without dc-link voltage control.

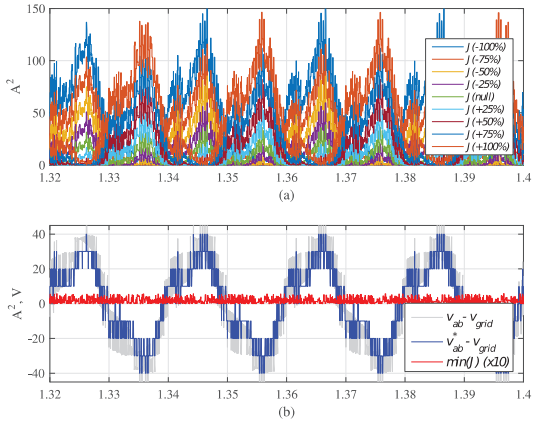

Fig. 9. Cost function components and voltage deviations related to Fig. 7 - with dc-link voltage control.

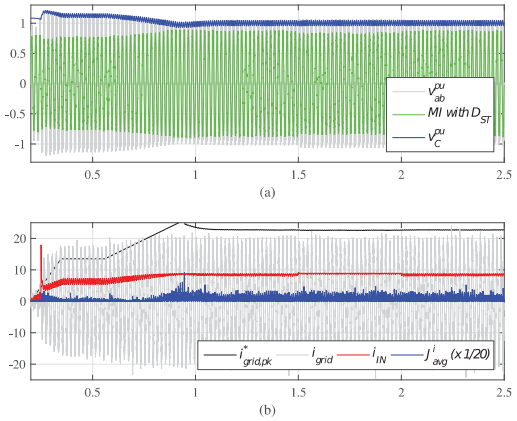

Fig. 10. Transient-time responses observed on voltage and current waveforms before and after dc-link voltage regulation.

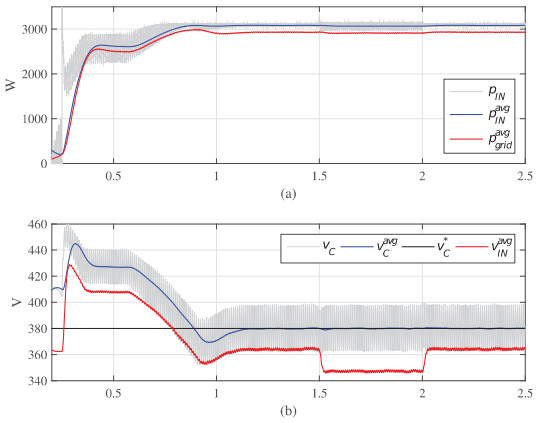

Fig. 11. Transient-time responses observed on power and voltage waveforms before and after dc-link voltage regulation.

Figs. 8 and 9 detail the operation of proposed indirect CCSMPC controller during the elaboration of reference voltage v_{ab}*. All possible finite values considered in (11) in terms of voltage v_{ab} range were compared to each other and a minimum cost function value was identified. Finally, an optimization of the cost function at every single simulation step provided square current error values closed to zero and, consequently, a proper regulation of grid current i_{grid}.

C. *Long-time observation window*

In terms of transient-time responses and rejection capability of the system for external perturbation signals, a long-time observation window was considered to verify these features. Then, Figs. 10 and 11 present some long-time waveforms from critical variables related to PV grid-connected system (Fig. 1).

By them it is possible to check that grid-connection was established at t = 0.2 s. Then, reference grid power p_{grid}* increased linearly until reaching a mid-power level (2.2 kW) almost 0.15 s later. And, finally, an external voltage loop control was enabled at t = 0.56 s. As it was expected from the control tuning method proposed in [13], a damped transient response of average dc-link voltage v_C lead it to settle over its reference value (380 V), achieved around 0.6 s later. During this time interval, grid reference current i_{grid}* increased and the proposed indirect CCS-MPC was still able to compensate grid current i_{grid} waveform and its variations.

Simultaneously, Fig. 11 also shows the dynamics of applied PV array model in response to external voltage control loop regulation. Combined dynamic actions resulted on a dc input voltage v_{IN} equals to 363 V, which it was lower than v_C* and close to MPP of PV array. A stable operation from that external loop was able just because the proposed indirect CCS-MPC was also able to provide the required waveform for i_{grid}*.

From Fig. 11 it is also possible to observe step variations on dc input voltage v_{IN} at t = 1.5 s and t = 2.0 s. Both step variations correspond to forced modifications on ST duty cycle, simulating a changing of exposition from PV modules to a new weather condition. Even during the worst case (low dc

input voltage profile), the dc-link voltage controller was able to keep the voltage v_C closed to its reference value and without any overshoot. As it depends on the inner grid control loop, the performance of proposed method was also verified.

V. Conclusion

In this paper, an indirect current CCS-MPC method was proposed in order to regulate the grid current provided by a grid-connected single-phase 3L-NPC qZS PV inverter. The proposed method is associated with discrete-time control systems and it was described in terms of its key control issues: internal dynamic model; cost function; considered constraints; optimization stage; and receding horizon length.

In order to reduce the difference between grid reference and current waveforms, the applied cost function and optimization stage were based on the lowest value of square current error provided by a fixed amount of ac output voltages. These issues were checked after every single discrete-time step for providing the most suggestive modulation index for 3L-NPC inverter before the next optimization checking.

Based on a simulation model built on PSCAD/EMTDC, an evaluation of the indirect current CCS-MPC method was discussed in terms of obtained simulation results. By different levels of power and operational conditions, it was verified the accuracy of proposed internal model and the robustness of proposed indirect CCS-MPC method. Both features correspond to an achievement of expected control objectives even under dynamic operating conditions and they validate the proposal.

During the evaluation of proposed method, authors identified that parameter R_f from IDM model (Fig. 3) has a huge influence on the control accuracy. It was noticed that higher values of R_f result on a better attenuation of voltage oscillations at capacitor C_f and, for that reason, allow a better tracking of sinusoidal reference waveforms.

Acknowledgment

This research was supported by the Estonian Centre of Excellence in Zero Energy and Resource Efficient Smart Buildings and Districts, ZEBE, grant 2014-2020.4.01.15-0016 funded by the European Regional Development Fund and co-supported by Estonian government PUT1443, PSG142, and MOBJD126.

References

[1] S. Kouro, J. I. Leon, D. Vinnikov, and L. G. Franquelo, "Grid-connected photovoltaic systems: An overview of recent research and emerging pv converter technology," *IEEE Industrial Electronics Magazine*, vol. 9, no. 1, pp. 47–61, March 2015.

[2] Y. Huang, M. Shen, F. Z. Peng, and J. Wang, "z-source inverter for residential photovoltaic systems," *IEEE Transactions on Power Electronics*, vol. 21, no. 6, pp. 1776–1782, Nov 2006.

[3] J. Rodriguez and P. Cortes, *Predictive Control of Power Converters and Electrical Drives*. Wiley-IEEE Press, 2012.

[4] T. Geyer, *Model Predictive Control of High Power Converters and Industrial Drives*. John Wiley & Sons Inc, 2016.

[5] C. Bordons and C. Montero, "Basic principles of MPC for power converters: Bridging the gap between theory and practice," *IEEE Industrial Electronics Magazine*, vol. 9, no. 3, pp. 31–43, sep 2015.

[6] S. Vazquez, R. P. Aguilera, P. Acuna, J. Pou, J. I. Leon, L. G. Franquelo, and V. G. Agelidis, "Model predictive control for single-phase NPC converters based on optimal switching sequences," *IEEE Transactions on Industrial Electronics*, vol. 63, no. 12, pp. 7533–7541, dec 2016.

[7] A. A. Ahmed, B. K. Koh, and Y. I. Lee, "A comparison of finite control set and continuous control set model predictive control schemes for speed control of induction motors," *IEEE Transactions on Industrial Informatics*, vol. 14, no. 4, pp. 1334–1346, April 2018.

[8] O. Husev, C. Roncero-Clemente, E. Romero-Cadaval, D. Vinnikov, and S. Stepenko, "Single phase three-level neutral-point-clamped quasi-zsource inverter," *IET Power Electronics*, vol. 8, no. 1, pp. 1–10, 2015.

[9] O. Husev, C. Roncero-Clemente, E. Romero-Cadaval, D. Vinnikov, and T. Jalakas, "Three-level three-phase quasi-z-source neutral-pointclamped inverter with novel modulation technique for photovoltaic application," *Electric Power Systems Research*, vol. 130, 2016.

[10] M. S. Fadali and A. Visioli, *Digital Control Engineering*. Elsevier Science Publishing Co Inc, 2012.

[11] M. Rivera, V. Yaramasu, A. Llor, J. Rodriguez, B. Wu, and M. Fadel, "Digital predictive current control of a three-phase four-leg inverter," *IEEE Transactions on Industrial Electronics*, vol. 60, no. 11, pp. 4903-4912, Nov 2013.

[12] L. R. A. Pinto, S. P. Pimentel, E. G. Marra, B. Alvarenga, T. M. Cesar, and C. K. D. Lima, "Proposal of model predictive control (mpc) method for a three-phase four-leg inverter applied in a distributed generation system," in *2017 Brazilian Power Electronics Conference (COBEP)*, Nov 2017, pp. 1–6.

[13] S. P. Pimentel, O. Husev, D. Vinnikov, C. Roncero-Clemente, E. Makovenko, and S. Stepenko, "Voltage control tuning of a singlephase grid-connected 3l qzs-based inverter for pv application," in *2018 IEEE 38th International Conference on Electronics and Nanotechnology (ELNANO)*, Apr. 2018.

[14] C. Roncero-Clemente, E. Gonzlez-Romera, E. Romero-Cadaval, M. I. Milans-Montero, and V. Miambres-Marcos, "Pscad/emtdc model for photovoltaic modules with mppt based on manufacturer specifications," in *2013 International Conference-Workshop Compatibility and Power Electronics*, June 2013, pp. 69–74.

[15] BISOL, "Multicrystalline pv modules bmu 255-275 wp," 2018. [Online]. Available: http://www.bisol.com/en/products/pvmodules/bisol-premium-series-poly.html